JOURNAL OF SPACECRAFT AND ROCKETS
Vol. 41, No. 2, March–April 2004

Nonlinear Aeroelastic Analysis of a Deployable Missile Control Fin

Jae-Sung Bae*
Virginia Polytechnic Institute and State University, Blacksburg, Virginia 24061
Dae-Kwan Kim,† Won-Ho Shin,† and In Lee‡
Korea Advanced Institute of Science and Technology, Daejon 305-701, Republic of Korea
and
Seung-Ho Kim§
Korea Aerospace Industry, Gyungnam 664-942, Republic of Korea

The nonlinear aeroelastic characteristics of a deployable missile control fin have been investigated. Modes from free vibration analysis and a doublet-point method are used for the computation of supersonic unsteady aerodynamic forces. The minimum-state approximation is used to approximate the aerodynamic forces. The fictitious mass modal approach is applied to reduce the problem size and the computation time in the linear and nonlinear flutter analyses. For the nonlinear flutter analysis, the deployable hinge is represented by an asymmetric bilinear spring and is linearized using the dual-input describing function method. From the nonlinear flutter analysis, three different types of limit-cycle oscillations are observed in the wide range of airspeed over the linear flutter boundary. The aeroelastic characteristics of the missile control fin can become more stable due to the existence of the deployable hinge nonlinearity.

Nomenclature

A	=	limit-cycle oscillation (LCO) amplitude
B	=	LCO offset
b	=	reference length (half root chord)
C_1	=	viscous damping
F_c	=	coulomb friction
$\{F(s)\}$	=	Laplace transform of $\{f\}$
$[GC]$	=	generalized damping matrix
$[GK]$	=	generalized stiffness matrix
$[GM]$	=	generalized mass matrix
K_{eq}	=	equivalent hinge stiffness
$[K_n]$	=	stiffness matrix with structural nonlinearity
K_θ	=	linear deployable hinge stiffness
P	=	preload
U	=	airspeed or flight speed
U_{ref}	=	linear flutter speed (425 m/s) when Mach number is 2.0
$\bar{U}$	=	speed ratio (U/U_{ref})
$\{X(s)\}$	=	Laplace transform of $\{\eta(t)\}$
x_a	=	augmented state by aerodynamic approximation
α	=	root pitch angle
δ	=	freeplay $[(s_2 - s_1)/2]$
θ	=	deployable hinge angle
$[\phi]$	=	modal matrix

Introduction

DEPLOYABLE missile control fins (shown in Fig. 1) have been used primarily because of their advantages in packaging tube-launched projectiles during past decades. Allowing more efficient use of space, these fins are folded against the projectile body and are unfolded after launching. The deployable hinge of the fin has a complex configuration consisting of a torsional spring, a compression spring, and several stoppers. Because of manufacturing tolerances, the hinge is loosened and then contains some of concentrated structural nonlinearities such as freeplay, bilinear nonlinearity, offset piecewise linear, friction, hysteresis, and coulomb damping.

Aeroelastic phenomena, such as flutter, are dynamic instabilities that involve inertia, aerodynamics, and elastic forces of a flight vehicle. If aeroelastic problems occur in flight, flight vehicle structures may fail. Therefore, it is important to predict aeroelastic characteristics accurately to prevent aeroelastic instabilities.

During the past several decades, most aeroelastic investigations for flight vehicles have been carried out under the assumption of structural linearity. Under this assumption, the flutter characteristics can be easily obtained. However, the aeroelastic results under the assumption of structural linearity may not agree with the physical phenomena because real structures may have some structural nonlinearities.

Nonlinear aeroelastic characteristics are quite different from their linear characteristics. Typically, nonlinear aeroelastic responses include flutter, divergence, limit-cycle oscillation, and chaotic motion. Limit cycle oscillation (LCO) is a periodic oscillation consisting of one or a couple of frequencies, and chaotic motion is a nonperiodic oscillation. When a linear system becomes unstable, the amplitude of the response increases exponentially, whereas a nonlinear system has a bounded motion such as LCO or chaotic motion, which may occur below the linear flutter speed. Neither LCO nor chaotic motion causes the abrupt failure of a structure. However, these motions can cause a structure to be damaged by fatigue and can considerably affect the control systems of flight vehicles. Thus, the effects of structural nonlinearities on the aeroelastic characteristics of flight vehicles should be considered in the design stage.

In recent years, nonlinear aeroelastic analyses of an airfoil and a wing with concentrated nonlinearities have been performed by several investigators. Woolston et al.[1] analyzed a relatively simple system including freeplay, hysteresis, and cubic nonlinearity and showed that the LCO may occur below the linear flutter boundary. Laurenson and Trn[2] studied the flutter of a missile control surface with structural nonlinearities using the describing function method. Lee[3] developed an iterative scheme for multiple nonlinearities using

Received 7 March 2003; revision received 6 June 2003; accepted for publication 12 June 2003.

*Ph.D. Researcher, Department of Mechanical Engineering; jsbae@vt.edu.
†Graduate Research Assistant, Department of Aerospace Engineering.
‡Professor, Department of Aerospace Engineering; inlee@asdl.kaist.ac.kr. Senior Member AIAA.
§Senior Engineer, T-50 Structural Analysis Team, Sachon-City.

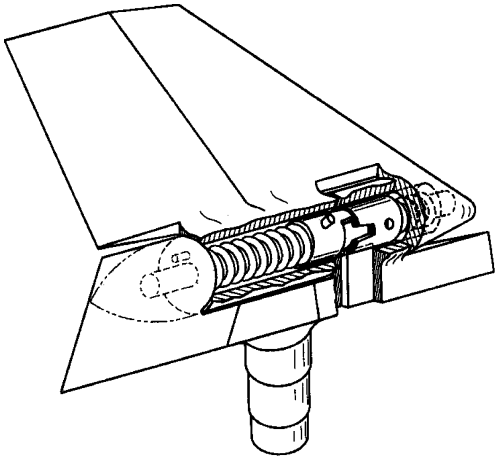

Fig. 1 Deployable missile control fin of K-SAM.

the describing function method and the structural dynamics modification technique. Lee and Tron[4] studied the flutter characteristics of CF-18 aircraft with structural nonlinearities in the leading-edge flap hinge and the wing-fold hinge using the describing function method. They considered both freeplay and bilinear nonlinearities. Yang and Zhao[5] studied the LCO of a typical section model with pitch nonlinearity subject to incompressible flow using the Theodorsen function. Lee and Kim[6] studied the LCO and chaotic motion of a missile control surface with freeplay nonlinearity using time-domain analysis. Conner et al.[7] studied the nonlinear behaviors of a typical section with control surface freeplay both numerically and experimentally. Paek et al.[8] studied the flutter characteristics of a wraparound fin considering rolling motion and aerodynamic nonlinearity. Recently, Bae et al.[9] studied the subsonic nonlinear flutter characteristics of a wing with a control surface using frequency-domain and time-domain analyses. Bae and Lee[10] studied the LCO characteristics of a missile control fin using a two-dimensional model with plunge and pitch modes and investigated the effects of the frequency ratio between plunge and pitch motions on the nonlinear aeroelastic characteristics. In Ref. 10, the authors showed that the LCOs can be observed below or over the linear flutter boundary, depending on the frequency ratio. Although Ref. 10 refers to a two-dimenstional model, this can provide the valuable information about the aeroelastic characteristics of a deployable missile control fin.

The purpose of the present study is to investigate the nonlinear aeroelastic characteristics of a deployable missile control fin. From dynamic test data, the nonlinearity of a deployable hinge is represented by an asymmetric bilinear spring using system identification. In the present study, the finite element method[11] is used for the free vibration analysis and doublet-point method (DPM)[12] is used for the computation of supersonic unsteady aerodynamic forces. Karpel's method[13] is used to approximate the unsteady aerodynamic forces. The fictitious mass method (FM)[14] is used to reduce the problem size and the computation time requirement. The effects of the nonlinear hinge on the nonlinear aeroelastic characteristics of a deployable missile control fin are investigated.

Theoretical Analysis

Aeroelastic Equation

The aeroelastic equation with a concentrated structural nonlinearity can be written as

$$[M]\{\ddot{u}\} + [C]\{\dot{u}\} + [K_n(u)]\{u\} = \{F(t, u, \dot{u})\} \tag{1}$$

where $[M]$, $[C]$, $\{F\}$, and $\{u\}$ are the mass matrix, damping matrix, aerodynamic force vector, and deflection vector, respectively. For a piecewise nonlinearity, the restoring force term, $[K_n(u)]\{u\}$, can be written as follows:

$$[K_n(u)]\{u\} = [K]\{u\} + \{f(u)\} \tag{2}$$

where $[K]$ is a linear stiffness matrix without a structural nonlinearity and $\{f(u)\}$ is the restoring force vector whose elements are zero except for the nonlinear contribution.

Generally, aeroelastic analysis is conducted in the generalized modal coordinate to save computational time and memory. In an aeroelastic system with structural nonlinearities, structural properties vary with motion. Hence, aeroelastic analysis using the constant modal coordinate of the nominal structure can give inaccurate results and may require a relatively large number of modes to achieve a reasonable level of accuracy. To overcome this problem, the FM method is used here. The basic idea of the FM method is that the local deformation due to the large added mass enables us to examine the structural variations such as structural nonlinearity. This method is an efficient and easy-to-apply computational scheme. References 9 and 14 can be referred to for a detailed description of the FM method.

When the modal matrix $[\phi]$obtained from the FM model is used, the structural displacements can be transformed into modal coordinates as follows:

$$\{u\} = [\phi]\{\eta\} \tag{3}$$

where $\{\eta\}$ is the displacement in modal coordinates. Then, the generalized aerodynamic forces can be written as

$$\{\bar{F}\} = [\phi]^T\{F\} = q[\phi]^T[Q][\phi]\{\eta\} = q[\bar{Q}]\{\eta\} \tag{4}$$

where $q(=\frac{1}{2}\rho U^2)$ and $[\bar{Q}]$ are dynamic pressure and the generalized aerodynamic coefficient matrix, respectively.

When the transformation in Eq. (3) is used, the aeroelastic equation in Eq. (1) can be transformed into the generalized coordinate as follows:

$$[GM]\{\ddot{\eta}\} + [GC]\{\dot{\eta}\} + [GK]\{\eta\} = q[\bar{Q}]\{\eta\} - [\phi]^T\{f(u)\} \tag{5}$$

State-Space Equations

To integrate the aeroelastic equations in Eq. (5), Eq. (5) may be transformed into state-space equations. Generally, the generalized aerodynamic influence coefficients are calculated for tabulated reduced frequencies k by unsteady aerodynamic methods such as computational fluid dynamics and DPM. Thus, the generalized aerodynamic influence coefficients should be approximated by a rational function. There are many methods for rational function approximation (RFA), such as Roger's RFA[15] and Karpel's minimum-state approximation (MSA),[13] and Karpel's MSA is used here. The approximation form of MSA is as follows:

$$[\bar{Q}(s)] = [P_1](b/U)^2s^2 + [P_2](b/U)s + [P_3] + [D](s[I] - [\bar{R}])^{-1}[E]s \tag{6}$$

where $[P_i]$, $[D]$, and $[E]$ are calculated from a least-square fit and $[\bar{R}]$ is a diagonal matrix. The diagonal terms of $[\bar{R}]$ are the aerodynamic poles and constants to be determined for the best fit of $[\bar{Q}]$.

When Laplace transformation and MSA are used, Eq. (5) can be written as

$$([\bar{M}]s^2 + [\bar{C}]s + [\bar{K}])\{X(s)\} = [\bar{D}]\{X_a(s)\} - [\phi]^T\{F(s)\} \tag{7}$$

where

$$[\bar{M}] = [GM] - \tfrac{1}{2}\rho b^2[P_1] \tag{8a}$$

$$[\bar{C}] = [GC] - \tfrac{1}{2}\rho U b[P_2] \tag{8b}$$

$$[\bar{K}] = [GK] - \tfrac{1}{2}\rho U^2[P_3] \tag{8c}$$

$$[\bar{D}] = \tfrac{1}{2}\rho U^2[D] \tag{8d}$$

In Eq. (7), the state vector $\boldsymbol{X}_a(s)$ by the aerodynamic approximation is obtained as

$$\{X_a(s)\} = (s[I] - [\bar{R}])^{-1}[E]s\{X(s)\} \tag{9}$$

Defining the new state v as $\dot{\eta}$, the final state-space aeroelastic equations are obtained as

$$\begin{Bmatrix} \dot{v} \\ \dot{\eta} \\ \dot{x}_a \end{Bmatrix} = \begin{bmatrix} -[\bar{M}]^{-1}[\bar{C}] & -[\bar{M}]^{-1}[\bar{K}] & -[\bar{M}]^{-1}[\bar{D}] \\ [I] & [0] & [0] \\ [E] & [0] & [\bar{R}] \end{bmatrix} \begin{Bmatrix} v \\ \eta \\ x_a \end{Bmatrix} + \begin{Bmatrix} -[\bar{M}]^{-1}[\phi]^T\{f\} \\ 0 \\ 0 \end{Bmatrix} \tag{10}$$

Method of Aeroelastic Analysis

The nonlinear aeroelastic analysis can be subdivided into two methods. One is the frequency-domain analysis such as the root-locus method, V–g method, and P–K method.[11] The other is the time-domain analysis, such as the time integration of Eq. (10). The frequency-domain and the time-domain methods have different approaches, whereas these methods give similar solutions for a linear aeroelastic problem. Therefore, it is efficient to use the frequency-domain analysis only for a linear problem. For a nonlinear problem, the frequency-domain analysis can give us inaccurate results, and the time-domain analysis is necessary.[8] The time-domain analysis requires much more computational time and effort to find an aeroelastic response such as LCO or chaotic motion. Moreover, it may be very difficult to find unstable LCO. Therefore, for a nonlinear problem, the frequency-domain analysis is conducted first, and then, based on the frequency-domain results, it is efficient to find the aeroelastic responses.[9]

In the present study, the root-locus method and the time-integration method are used for nonlinear aeroelastic analysis. The root-locus method involves tracing the root loci of Eq. (10). As the airspeed U is increased, a real part eigenvalue of Eq. (10) is changed from negative to positive. This point is the flutter point, and the speed U is the flutter speed U_f. The Runge–Kutta method is used to integrate Eq. (10).

Nonlinear Model of Deployable Hinge

It is difficult, dangerous, and expensive to conduct flutter experiments of nonlinear systems in a wind tunnel or a flight test. Over the past several decades, a number of researchers have verified the accuracy of the aeroelastic analysis method for most cases, except those involving very complex structures. Figure 2 shows a road map for the present nonlinear aeroelastic analysis of a missile control fin and the flutter analysis and the experiment combined. From the dynamic test of a deployable missile control fin, the existence of structural nonlinearities can be identified, and the nonlinear hinge model can be established by using a force-state mapping technique.[16] Figure 3

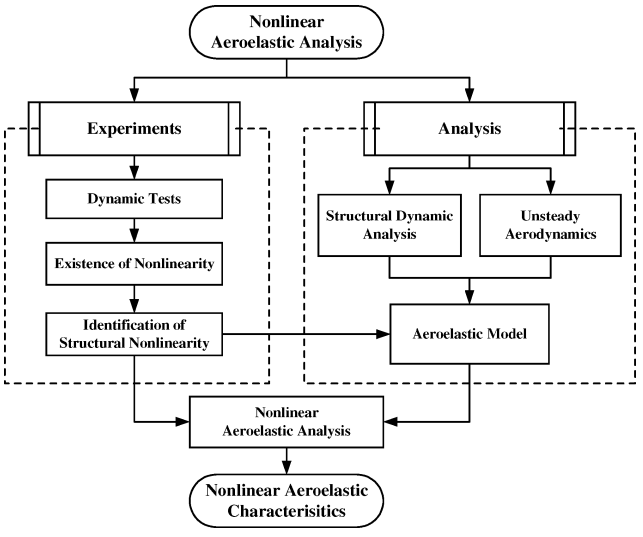

Fig. 2 Road map of nonlinear aeroelastic analysis in the present study.

Table 1 Parameters of nonlinear hinge

Parameter	Value
δ	0.636 deg
s_1/δ	0.063
a_1	0.115
a_2	0.842
C_1	0.133 N · m · s/rad
F_c	0.200 N · m
P	−0.108 N · m
K_1	348.8 N · m/rad

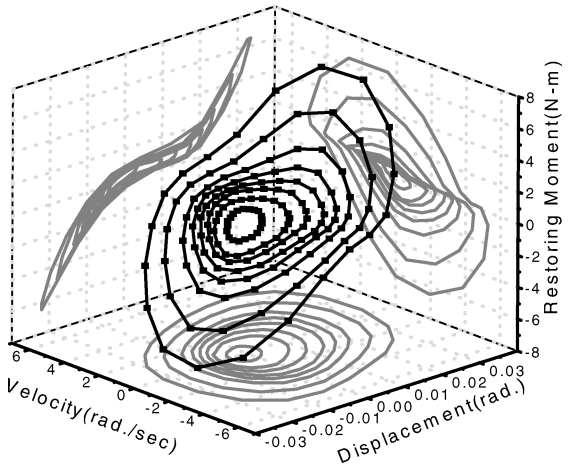

Fig. 3 Experimentally measured force-state map of nonlinear hinge (30 Hz).

shows the force-state map of the nonlinear hinge and several nonlinearities such as bilinear and freeplay are observed. The nonlinear restoring force $R(x, \dot{x})$ of the hinge can be represented as follows[17]:

$$R(x, \dot{x}) = P + C_1\dot{x} + F_c \operatorname{sign}(\dot{x}) + F_{\text{nonlinear}} \tag{11}$$

with

$$F_{\text{nonlinear}} = \begin{cases} K_1(x - s_1) & \text{for} \quad x < s_1 \\ K_2(x - s_1) & \text{for} \quad s_1 < x < s_2 \\ K_3(x - s_2) + K_2(s_2 - s_1) & \text{for} \quad s_2 < x \end{cases} \tag{12}$$

$$K_2 = a_1K_1, \qquad K_3 = a_2K_1 \tag{13}$$

where K_i and $(s_2 - s_1)/2$ are stiffness and freeplay, respectively. The nonlinear hinge of the fin has freeplay of 0.636 deg, and the stiffnesses of the folding and unfolding sides are different. Table 1 shows the parameters of a nonlinear hinge. Coulomb friction is existent but is negligible compared with other nonlinearities. Viscous damping decreases as the excitation frequency increases.[17]

When the viscous damping and coulomb damping in Eq. (11) are ignored, the nonlinear restoring force is dependent on the displacement, and the deployable hinge can be represented by an asymmetric bilinear spring as shown in Fig. 4. Relations between nonlinear restoring force and displacement can be written as

$$f(x) = \begin{cases} K_1x & \text{for} \quad x < s_1 \\ (K_1 - K_2)s_1 + K_2x & \text{for} \quad s_1 < x < s_2 \\ (K_1 - K_2)s_1 + (K_2 - K_3)s_2 + K_3x & \text{for} \quad s_2 < x \end{cases} \tag{13}$$

where x and $f(x)$ are a deployable hinge angle and a hinge moment, respectively.

For frequency-domain aeroelastic analysis, the equivalent stiffness of a nonlinear spring in Eq. (13) should be obtained. The

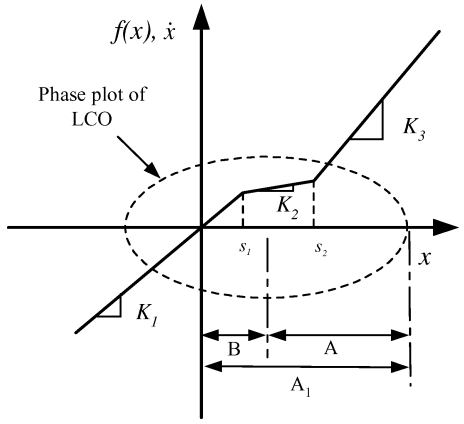

Fig. 4 Asymmetric bilinear spring.

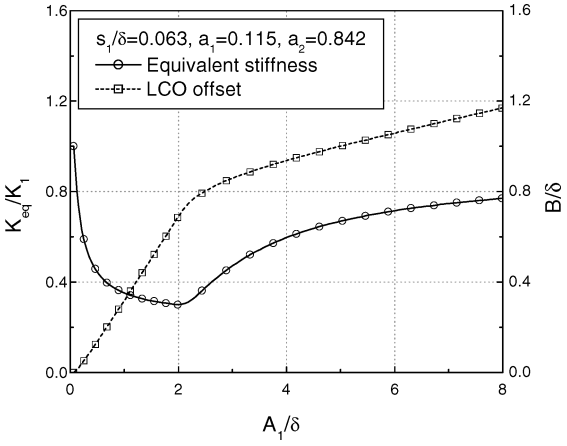

Fig. 5 Equivalent stiffness and LCO offset of an asymmetric bilinear spring.

describing function[2] can give us the method for obtaining the equivalent system of a nonlinear spring. Under the assumption of a harmonic motion, we can obtain the equivalent stiffness of a nonlinear spring using the describing function. To account for general cases such as the asymmetric bilinear spring shown in Fig. 4, a dual-input describing function technique[18,19] should be used, and so the equivalent stiffness of an asymmetric bilinear spring was derived in Ref. 10. Figure 5 shows the equivalent stiffness of a nonlinear spring used in the present study and points out the relation between LCO amplitude of an aeroelastic response and the equivalent stiffness of the nonlinear spring. As shown in Fig. 5, the equivalent stiffness decreases within freeplay and increases beyond freeplay as LCO amplitude increases. Thus, an asymmetric bilinear spring has both softening and hardening stiffness characteristics.[17]

Nonlinear Aeroelastic Analysis

The missile control fin of K-SAM shown in Fig. 1 is used for the aeroelastic analysis. Actually, a servoactuator is connected at its root, and some nonlinearities may exist on it. To investigate the effects of the deployable hinge only, it is assumed that the fin does not have any nonlinearity except for the deployable hinge and that the servoactuator is represented by a linear torsional spring whose stiffness is 350.3 N · m/rad. The air density used in the aeroelastic analysis is 1.225 kg/m^3.

Free Vibration Analysis

We need the generalized mass and stiffness matrices and the mode shapes of a deployable missile control fin for the aeroelastic analysis. In addition, we need to verify the FM method for the fin. In the present study, the finite element method (FEM)[11] is used for the free vibration analysis of the fin. Four-node plate elements and bar elements are used to model the lower/upper wings and the hinge structures, respectively. Rigid-bar elements and multipoint constraints are used to connect plate elements with bar elements. Two one-dimensional spring elements for a hinge spring and a root rotational spring are used. Two point mass elements are used for using the FM method. Figure 6 shows the FEM model of a deployable missile control fin.

Table 2 Comparison of natural frequencies; $K_\theta = K_1$

Mode number	Natural frequency, Hz	
	Direct	FM
1	130.02	130.02
2	179.23	179.23
3	1130.7	1130.8
4	1299.3	1300.5
5	2091.3	2091.4
6	2607.7	2613.6
7	3060.2	3060.4
8	3135.9	3193.1
9	3520.4	5009.6
10	3822.9	22162

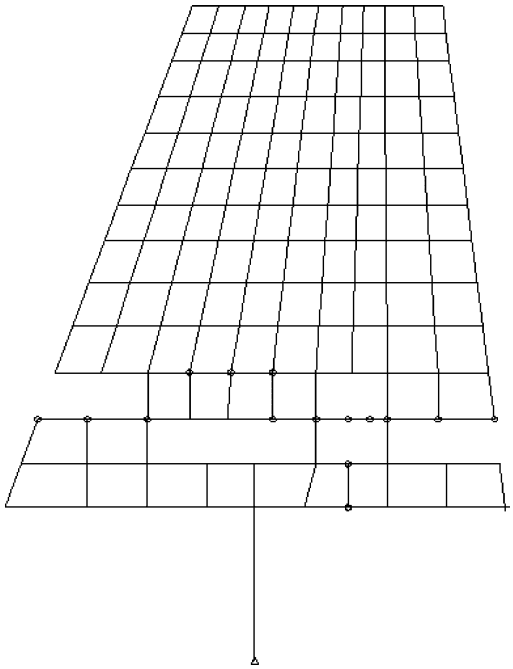

Fig. 6 FEM mesh of deployable missile control fin.

Table 2 shows the natural frequencies of the deployable missile control fin using both the direct method and the FM method when the hinge stiffness is K_1. With the direct method, the fin is directly modeled with a deployable hinge and a root spring, whereas with the FM method, it is with two FMs and without hinge and root springs. Through the free vibration analysis, the FM model is established by adding hinge and root springs.[14] Natural frequencies of the FM method are in good agreement with those of the direct model, except for the highest two modes. Figure 7 shows the lowest four modes of the missile control fin. The first-mode is the deployable mode of an upper wing and the second mode is the rigid pitching mode. The frequency ratio between the first mode and the second mode is 0.725. The third and fourth modes are the higher flexible modes of the upper wing.

Linear and Nonlinear Aeroelastic Analysis

The present aeroelastic analysis method is verified before the linear and nonlinear aeroelastic analyses of a deployable missile control fin. A linear aeroelastic analysis for the fin is performed using a hinge stiffness of 348.8 N · m/rad. The DPM code[17] is used to

compute the supersonic unsteady aerodynamic forces and a 10×8 mesh is used for the aerodynamic computation. This method is to calculate the relation between the pressure difference at the doublet point and the downwash at the receiving point using a kernel function.[12] The number of modes used for the aeroelastic analysis is 12. The results of the present aeroelastic analysis are compared with those obtained using Ref. 11, which uses the DPM and KE method. Comparison of the flutter speeds and frequencies with various methods is shown in Table 3. The results of the V–g method, root-locus method, and time-integration method are in good agreement with those using Ref. 11. The results of the FM method are very accurate compared with those of the direct method.

From the linear aeroelastic characteristics, we can infer the nonlinear aeroelastic characteristics such as the nonlinear flutter boundary. Hence, the effects of a hinge stiffness variation on the aeroelastic characteristics are investigated. Figure 8 shows the linear aeroelastic characteristics of the deployable missile control fin when Mach number is 2.0. The flutter speed increases as the hinge stiffness decreases, whereas the flutter frequency decreases. The flutter type is first–second mode coalescent flutter. The reason for the increasing flutter speed is that the first mode goes far from the second mode due to the decreases in the hinge stiffness. As shown in Fig. 5, the stiffness of a nonlinear hinge decreases due to the structural nonlinearity. In Ref. 10 it is shown that LCOs are observed over the linear flutter boundary when the frequency ratio is smaller than 1.0. The frequency ratio of the present model is 0.725. Therefore, the nonlinear flutter speed of the deployable missile control fin will be expected to increase compared with the linear flutter speed.

Figures 9–11 show the three types of LCOs when $\bar{U}$ is 1.2. The type of LCO is dependent on the initial condition. LCOs shown in Figs. 9 and 11 are stable LCO with small amplitude and unstable LCO with large amplitude, respectively, whereas their frequencies (157.4 Hz) and LCO flutter mode shapes are the same. Stable LCO is a stable oscillation, which remains independent of initial conditions and cannot affect the stability of an aeroelastic system, whereas unstable LCO appears in the transient region and eventually migrates to another aeroelastic response such as stable LCO or divergent flutter. For the amplitude ratios of LCOs shown in Figs. 9 and 11, the equivalent stiffness of a nonlinear hinge is about 0.735 and two different types of LCOs dependent on the path can be predicted from Fig. 8. The line and dash arrows in Fig. 8 show the path of the aeroelastic responses such as stable LCO and unstable LCO as the amplitude ratio shown in Fig. 5 increases. For stable LCO, if the amplitude of LCO increases due to disturbances; the stiffness ratio decreases and the flutter speed increases. Hence, the response cannot grow and goes back to the original motion. However, if the amplitude decreases, the stiffness ratio increases and the flutter speed decreases. Then the response goes to the original motion. For unstable LCO, if the amplitude increases, the stiffness ratio increases, and the flutter speed decreases. Hence, the response grows and becomes unstable. If the amplitude decreases, the stiffness ratio decreases, and the flutter speed increases. Accordingly, the response goes to stable LCO. Thus, stable LCO remains, whereas unstable LCO does not remain and goes to different motions.

Table 3 Comparison of flutter speeds and frequencies; $M = 2.0$ and $K_\theta = K_1$

Method	Flutter speed, m/s	Flutter frequency, Hz
V–g (direct)	424.4	162.8
Root locus (direct)	424.7	162.8
V–g (FM)	424.4	162.8
Root locus (FM)	424.7	162.8
Time (FM)	425.4	162.5
NASTRAN (KE, DPM)	433.2	161.5

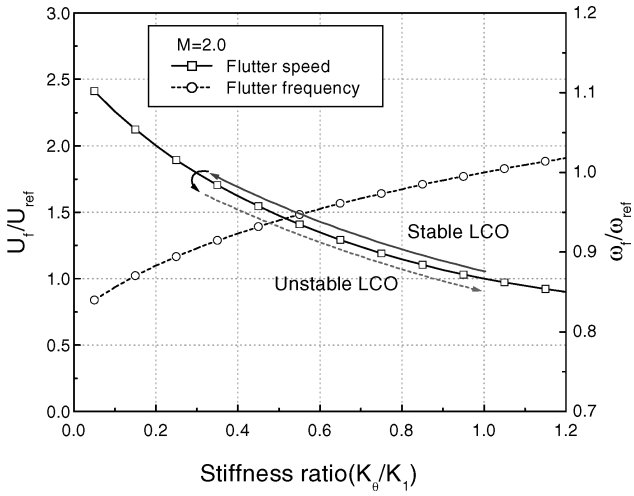

Fig. 8 Effects of K_θ on linear flutter characteristics.

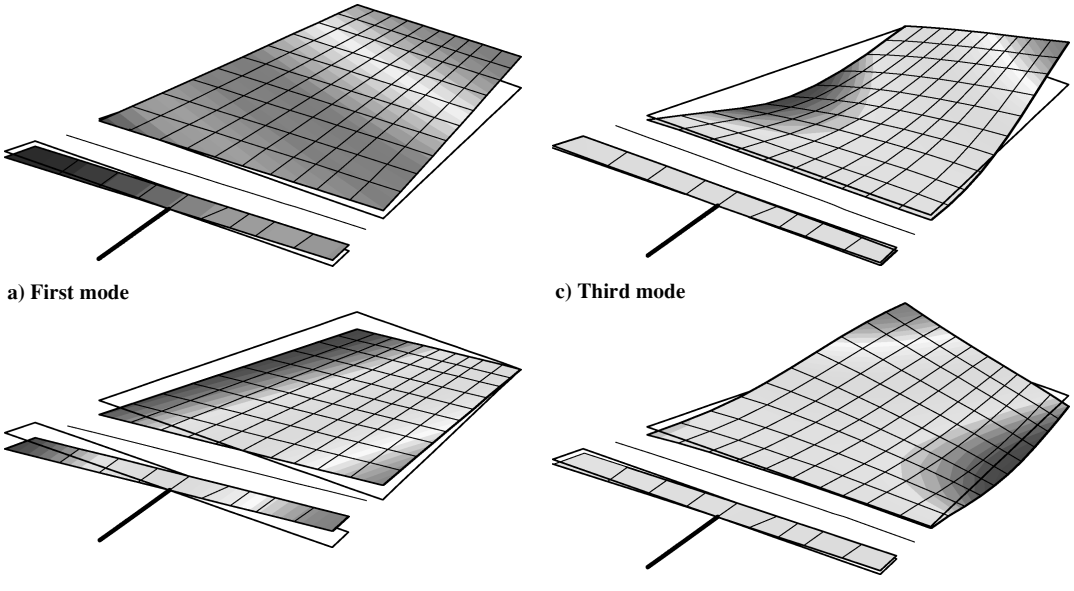

a) First mode **c) Third mode**

b) Second mode **d) Fourth mode**

Fig. 7 Mode shapes of deployable missile control fin; $K_\theta = K_1$.

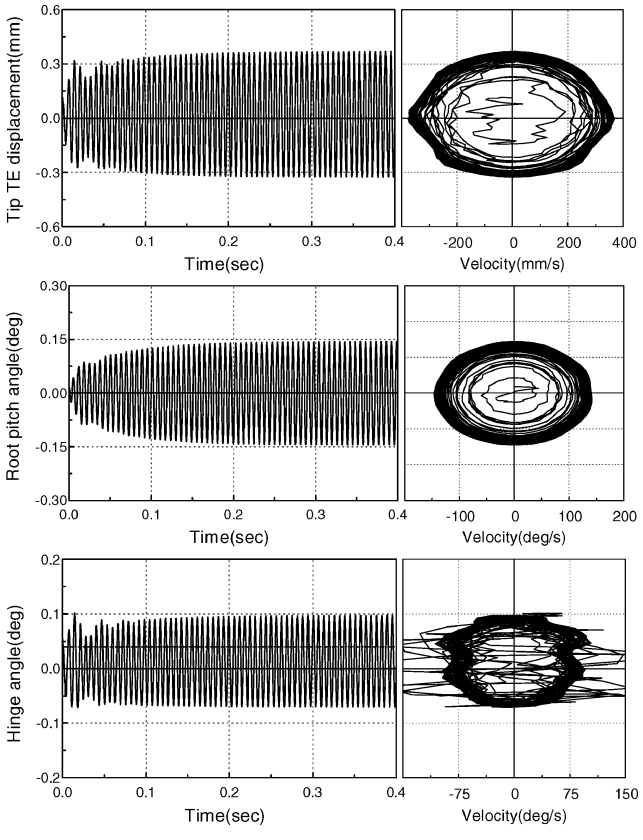

Fig. 9 Time history and phase plot; $\bar{U} = 1.2$ and $\theta_0/\delta = 0.1$.

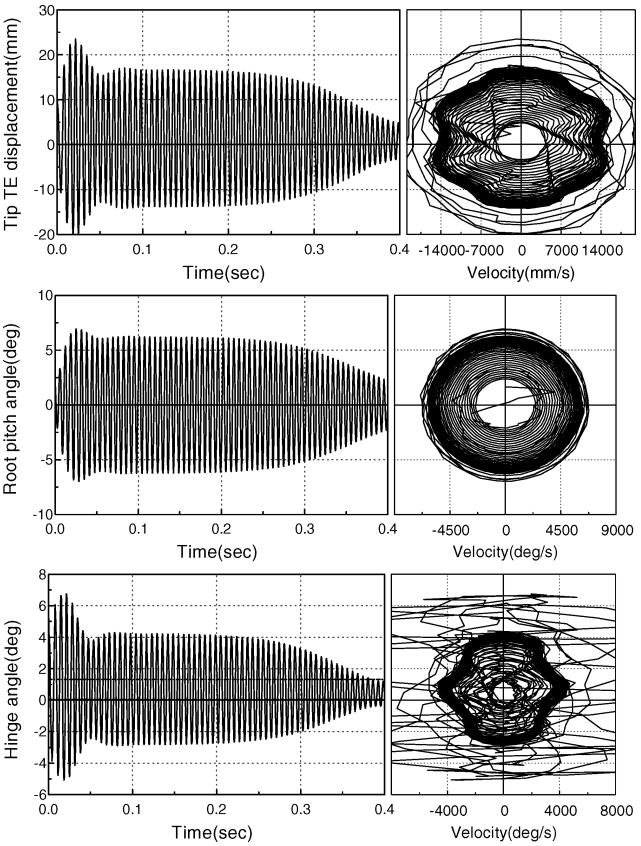

Fig. 11 Time history and phase plot; $\bar{U} = 1.2$ and $\theta_0/\delta = 8.8$.

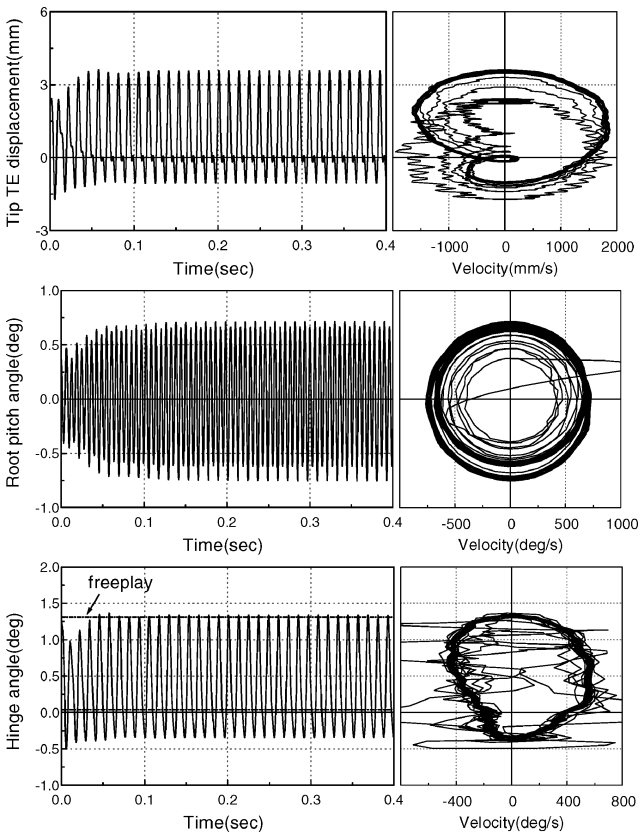

Fig. 10 Time history and phase plot; $\bar{U} = 1.2$ and $\theta_0/\delta = 2.0$.

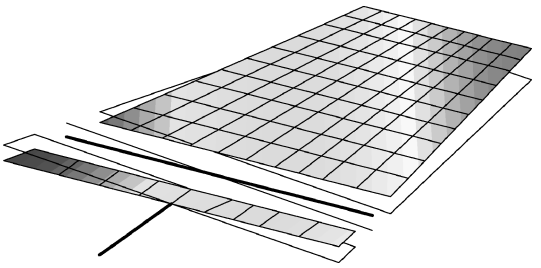

Fig. 12 LCO flutter mode shape of stable LCO.

Figure 12 shows the LCO flutter mode shape of a stable LCO, and the LCO mode is the first–second (deployable–pitching) coalescent mode. As shown in Fig. 11, a large-amplitude LCO transiently occurs and disappears, and then a small-amplitude LCO remains. When the initial condition (θ_0/δ) is greater than 8.8, the aeroelastic responses becomes unstable. The LCO shown in Fig. 10 is different from others and has the low frequencies with 82.5 Hz of a hinge and 167.4 Hz of a root. This LCO mode is not the first–second coalescent mode, but the first mode (deployable mode) and the second mode (rigid pitching mode) remain independent.

Figure 13 shows the hinge amplitude of LCO, and the different types of LCO are observed in the range of airspeed over the linear flutter speed. Both stable and unstable LCOs are predicted in the frequency-domain analysis, whereas the unpredicted LCO shown in Fig. 10 is observed only in the time-domain analysis. The hinge amplitude of unpredicted LCO is about 2δ. When the hinge amplitude is 2δ, the equivalent stiffness has a minimum value as shown in Fig. 5, but the linear flutter speed has maximum value as shown in Fig. 8. The unpredicted LCO could not be predicted in the linear flutter analysis and the nonlinear frequency-domain analysis. In Ref. 10, the unpredicted LCO could not be observed. This LCO is likely to be caused by the flexible modes or the nonlinear characteristics

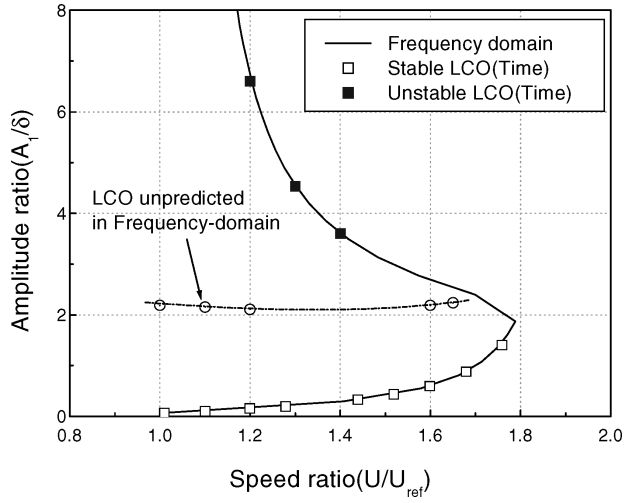

Fig. 13 LCO amplitudes vs air speeds.

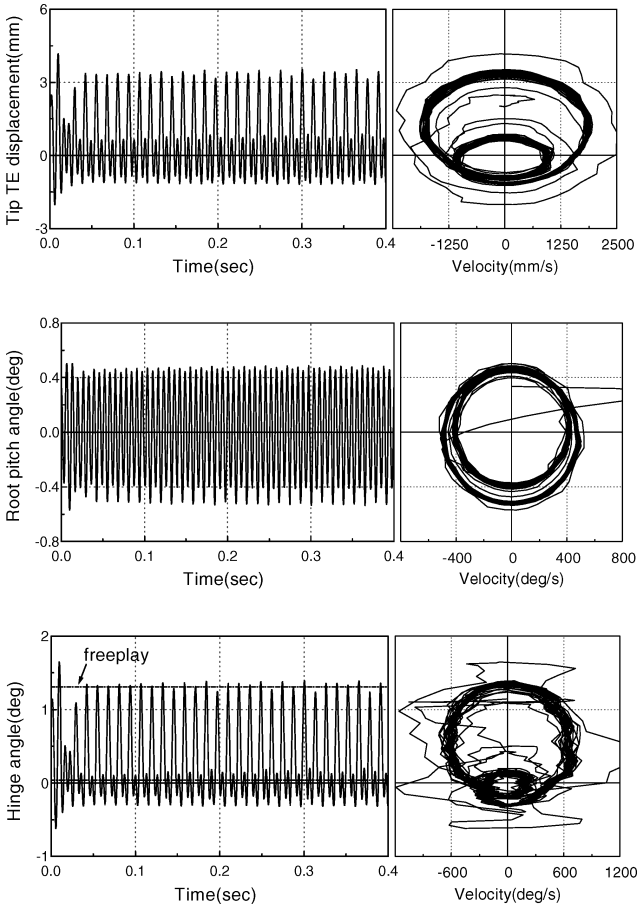

Fig. 14 Time history and phase plot; $\bar{U} = 1.6$ and $\theta_0/\delta = 1.8$.

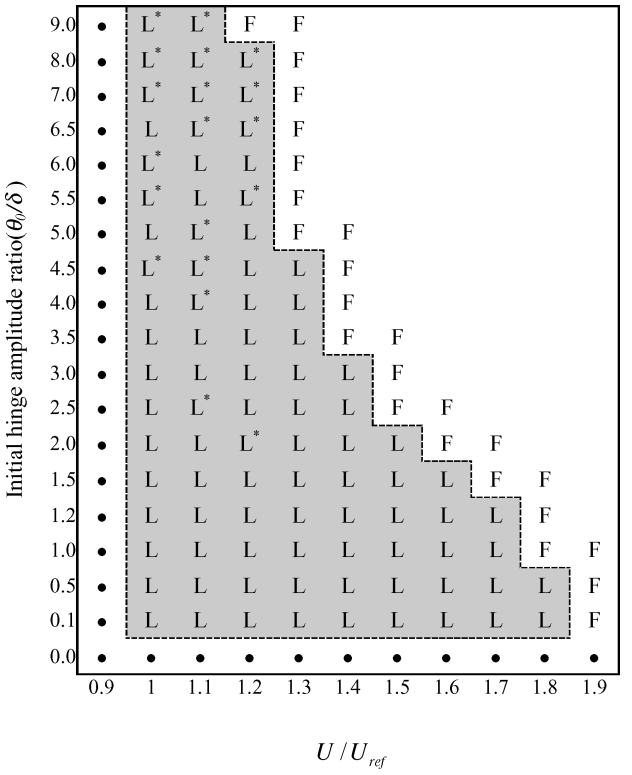

Fig. 15 Parameter map of deployable missile control fin: ●, damped stable motion; L, LCO; L, unpredicted LCO; and F, divergent fluttter.

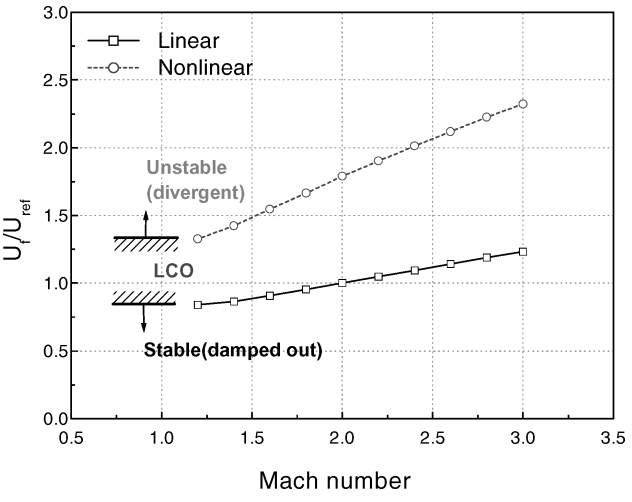

Fig. 16 Linear and nonlinear flutter boundaries of deployable missile control fin.

of the fin. Figure 14 shows the complicated motion with two different LCO amplitudes at the boundary of divergent flutter. One is a stable LCO (154.9 Hz), and the other is an unpredicted LCO (77.5 Hz).

Figure 15 shows a parameter map, which shows the types of aeroelastic responses for various speed ratios and initial amplitude ratios. When the speed ratio is greater than 1.0, LCOs or divergent aeroelastic responses are observed, depending on an initial amplitude ratio. The unstable LCOs shown in Fig. 11 are mainly observed at the boundary between stable LCOs and divergent flutter. For special initial amplitudes, the unpredicted LCO shown in Fig. 10 can be observed.

Figure 16 shows the linear and nonlinear flutter boundaries of a deployable missile control fin. As shown in Fig. 16, LCOs are observed at the wide range of airspeeds over the linear flutter boundary, and the nonlinear flutter boundary increases by the hinge nonlinearity of the fin. The region of LCO expands as the Mach number increases. Figure 17 shows the linear and nonlinear aeroelastic responses at the linear flutter speed. For the same initial condition, the amplitude of the nonlinear aeroelastic response is smaller than that of the linear aeroelastic response. Thus, due to the nonlinearity of a deployable hinge, the flutter boundary of the missile control fin increases, and also the amplitudes of stable LCOs are small, as shown in Fig. 13.

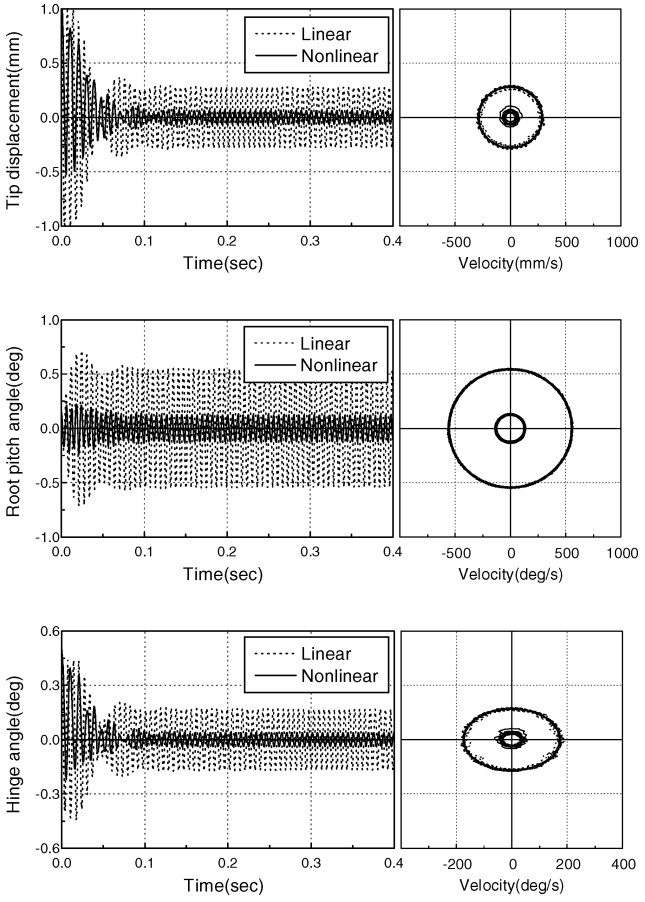

Fig. 17 Linear and nonlinear aeroelastic responses; $\bar{U} = 1.0$ and $\theta_0/\delta = 0.8$.

Therefore, we can conclude that the hinge nonlinearity causes the aeroelastic characteristics of the fin to become more stable.

Conclusions

Nonlinear aeroelastic analyses of the deployable missile control fin are performed in the frequency domain and the time domain. The results of the free vibration analysis and linear flutter analysis support the validity of the present method. Nonlinearity of a deployable hinge spring is represented by an asymmetric bilinear nonlinearity, and the dual-input describing function method is used for the frequency-domain analysis. Because of the hinge nonlinearity, the equivalent stiffness of the hinge spring decreases considerably. This causes the increases of the linear flutter speeds because the first mode of the fin goes far from the second mode.

From the nonlinear aeroelastic analyses, LCOs with different amplitudes are observed in a wide range of airspeeds over the linear flutter boundary. The type of LCO is dependent on the initial condition, and the aeroelastic responses can be made unstable by the initial condition. A stable LCO has a small amplitude, and the nonlinear aeroelastic boundary increases compared with the linear aeroelastic boundary. Thus, because of the nonlinearity of a deployable hinge, the aeroelastic characteristics of the deployable missile control fin can become more stable than with the linear case.

Acknowledgments

This research was supported by the Agency for Defense Development and was partially supported Ministry of Science and Technology (National Research Laboratory Program) of the Republic of Korea. This support is gratefully acknowledged.

References

[1]Woolston, D. S., Runyan, H. W., and Andrews, R. E., "An Investigation of Effects of Certain Type of Structural Nonlinearities on Wing and Control Surface Flutter," *Journal of the Aeronautical Sciences*, Vol. 24, Jan. 1957, pp. 57–63.

[2]Laurenson, R. M., and Trn, R. M., "Flutter Analysis of Missile Control Surface Containing Structural Nonlinearities," *AIAA Journal*, Vol. 18, No. 10, 1980, pp. 1245–1251.

[3]Lee, C. L., "Iterative Procedure for Nonlinear Flutter Analysis," *AIAA Journal,* Vol. 24, No. 5, 1986, pp. 833–840.

[4]Lee, B. H. K., and Tron, A., "Effects of Structural Nonlinearities on Flutter Characteristics of the CF-18 Aircraft," *Journal of Aircraft*, Vol. 26, No. 8, 1989, pp. 781–786.

[5]Yang, Z. C., and Zhao, L. C., "Analysis of Limit Cycle Flutter of an Airfoil in Incompressible Flow," *Journal of Sound and Vibration*, Vol. 123, No. 1, 1988, pp. 1–13.

[6]Lee, I., and Kim, S. H., "Aeroelastic Analysis of a Flexible Control Surface with Structural Nonlinearity," *Journal of Aircraft*, Vol. 32, No. 4, 1995, pp. 868–874.

[7]Conner, M. D., Tang, D. M., Dowell, E. H., and Virgin, L. N., "Nonlinear Behavior of a Typical Airfoil Section with Control Surface Freeplay: A Numerical and Experimental Study," *Journal of Fluid and Structures*, Vol. 11, No. 1, 1997, pp. 89–109.

[8]Paek, S. H., Bae, J. S., and Lee, I., "Flutter Analysis of a Wraparound Fin Projectile Considering Rolling Motion," *Journal of Spacecraft and Rockets*, Vol. 39, No. 1, 2002, pp. 66–72.

[9]Bae, J. S., Yang, S. M., and Lee, I., "Linear and Nonlinear Aeroelastic Analysis of a Fighter-Type Wing with Control Surface," *Journal of Aircraft*, Vol. 39, No. 4, 2002, pp. 697–708.

[10]Bae, J. S., and Lee, I., "Limit Cycle Oscillation of Missile Control Fin with Structural Nonlinearity," *Journal of Sound and Vibration* (to be published).

[11]"MSC/NASTRAN User's Manual," MacNeal–Schwendler Corp., Los Angeles, 1981.

[12]Ueda, T., and Dowell, E. H., "Doublet Point Method for Supersonic Unsteady Lifting Surfaces," *AIAA Journal*, Vol. 22, No. 2, 1984, pp. 179–186.

[13]Karpel, M., "Design for Active Flutter Suppression and Gust Alleviation Using State-Space Aeroelastic Modeling," *Journal of Aircraft*, Vol. 19, No. 3, 1982, pp. 221–227.

[14]Karpel, M., and Newman, M., "Accelerated Convergence for Vibration Modes Using the Substructure Coupling Method and Fictitious Coupling Masses," *Israel Journal of Technology*, Vol. 13, Feb. 1975, pp. 55–62.

[15]Roger, K. L., "Airplane Math Modeling Methods for Active Control Design," AGARD Rept. 228, 1977.

[16]Crawley, E. F., and Aubert, A. C., "Identification of Nonlinear Structural Elements by Force-State Mapping," *AIAA Journal*, Vol. 24, No. 1, 1986, pp. 155–162.

[17]Bae, J. S., "Aeroelastic Characteristics and Flutter Suppression Considering Structural Nonlinearity," Ph.D. Dissertation, Dept. of Aerospace Engineering, Korea Advanced Inst. of Science and Technology, Daejeon, Republic of Korea, Aug. 2002.

[18]Gelb, A., and Vander Velde, W. E., *Multiple-Input Describing Functions and Nonlinear System Design*, McGraw–Hill, New York, 1986, pp. 250–288.

[19]Price, S. J., Alighanbari, H., and Lee, B. H. K., "The Aeroelastic Response of a Two-Dimensional Airfoil with Bilinear and Cubic Structural Nonlinearities," *Journal of Fluids and Structures*, Vol. 9, No. 2, 1995, pp. 175–193.

P. Weinacht
Associate Editor